Ⓔ

THE ULTRAVIOLET, OPTICAL, AND INFRARED PROPERTIES OF SLOAN DIGITAL SKY SURVEY SOURCES DETECTED BY *GALEX*

MARCEL A. AGÜEROS,[1,2] ŽELJKO IVEZIĆ,[1] KEVIN R. COVEY,[1] MIRELA OBRIĆ,[3] LEI HAO,[4] LUCIANNE M. WALKOWICZ,[1]
ANDREW A. WEST,[1] DANIEL E. VANDEN BERK,[5] ROBERT H. LUPTON,[6] GILLIAN R. KNAPP,[6] JAMES E. GUNN,[6]
GORDON T. RICHARDS,[6] JOHN BOCHANSKI, JR.,[1] ALYSON BROOKS,[1] MARK CLAIRE,[1] DARYL HAGGARD,[1]
NATHAN KAIB,[1] AMY KIMBALL,[1] STEPHANIE M. GOGARTEN,[1] ANIL SETH,[1] AND MICHAEL SOLONTOI[1]

ABSTRACT

We discuss the ultraviolet, optical, and infrared properties of the Sloan Digital Sky Survey (SDSS) sources detected by the *Galaxy Evolution Explorer* (*GALEX*) as part of its All-sky Imaging Survey Early Release Observations. Virtually all (>99%) the *GALEX* sources in the overlap region are detected by SDSS; those without an SDSS counterpart within our $6''$ search radius are mostly unflagged *GALEX* artifacts. *GALEX* sources represent $\sim$2.5% of all SDSS sources within these fields, and about half are optically unresolved. Most unresolved *GALEX*-SDSS sources are bright ($r < 18$ mag), blue, turnoff, thick-disk stars and are typically detected only in the *GALEX* near-ultraviolet (NUV) band. The remaining unresolved sources include low-redshift quasars ($z < 2.2$), white dwarfs, and white dwarf–M dwarf pairs, and these dominate the optically unresolved sources detected in both *GALEX* bands.

Almost all the resolved SDSS sources detected by *GALEX* are fainter than the SDSS main spectroscopic limit. (Conversely, of the SDSS galaxies in the main spectroscopic sample, about 40% are detected in at least one *GALEX* band.) These sources have colors consistent with those of blue (spiral) galaxies ($u - r < 2.2$), and most are detected in both *GALEX* bands. Measurements of their UV colors allow much more accurate and robust estimates of star formation history than are possible using only SDSS data. Indeed, galaxies with the *most recent* ($\lesssim$20 Myr) star formation can be robustly selected from the *GALEX* data by requiring that they be brighter in the far-ultraviolet (FUV) than in the NUV band. However, older starburst galaxies have UV colors similar to those of active galactic nuclei and thus cannot be selected unambiguously on the basis of *GALEX* fluxes alone. Additional information, such as spatially resolved FUV emission, optical morphology, or X-ray and radio data, is needed before blue *GALEX* colors can be unambiguously interpreted as a sign of recent star formation.

With the aid of Two Micron All Sky Survey data, we construct and discuss median 10-band UV through infrared spectral energy distributions for turnoff stars, hot white dwarfs, low-redshift quasars, and spiral and elliptical galaxies. We point out the high degree of correlation between the UV color and the contribution of the UV flux to the UV through infrared flux of galaxies detected by *GALEX*; for example, this correlation can be used to predict the SDSS *z*-band measurement, using only two *GALEX* fluxes, with a scatter of only 0.7 mag.

Key words: catalogs — galaxies: active — galaxies: starburst — ultraviolet: galaxies — ultraviolet: general — ultraviolet: stars

Online material: color figures

1. INTRODUCTION

Launched in 2003 April, the *Galaxy Evolution Explorer* (*GALEX*) made its first public data release (the Early Release Observations [ERO]) at the end of 2003. Included in the ERO are fields from several different *GALEX* surveys that overlap with the Sloan Digital Sky Survey (SDSS; York et al. 2000), allowing one to study sources over nearly the entire 1000–10000 Å range (see Fig. 1).[7] Here we report the results of matching *GALEX* All-sky Imaging Survey (AIS; $t_{\rm exp} \approx 100$ s) observations with

SDSS data in the overlapping fields. There are other, deeper *GALEX* observations of SDSS fields in the ERO, but AIS is the *GALEX* survey that will eventually provide the largest sky coverage.[8] It is therefore the most appropriate *GALEX* survey for discussing the bulk properties of objects in the overlapping *GALEX*-SDSS region.

We describe the optical properties of matched *GALEX*-SDSS sources in three AIS ERO fields, covering $\sim$3 deg^2 of sky, which overlap the SDSS first data release footprint. The first full *GALEX* public data release should contain about 1000 deg^2 of overlap with the SDSS (Seibert et al. 2005a) and therefore allow the construction of a much larger sample of matched objects than discussed in this paper. However, even the fairly small sample discussed here (about 3000 matched sources) is sufficient to highlight some of the challenges in producing a good sample of *GALEX*-SDSS sources and to characterize the optical SDSS properties of the matched sources, as well as to

---

[1] Department of Astronomy, University of Washington, Box 351580, Seattle, WA 98195; agueros@astro.washington.edu.
[2] NASA Harriett G. Jenkins Predoctoral Fellow.
[3] Kapteyn Institute, Postbus 800, Groningen 9700 AV, Netherlands.
[4] Department of Astronomy, Cornell University, 610 Space Sciences Building, Ithaca, NY 14853.
[5] Department of Physics and Astronomy, University of Pittsburgh, 3941 O'Hara Street, Pittsburgh, PA 15260.
[6] Princeton University Observatory, Princeton, NJ 08544.
[7] See http://www.galex.caltech.edu/EROWebSite/Early_release_data_description_part2.htm.

[8] The Medium Imaging Survey is $\sim$2.5 mag deeper and will cover about 1000 deg^2 of sky overlapping the SDSS footprint.
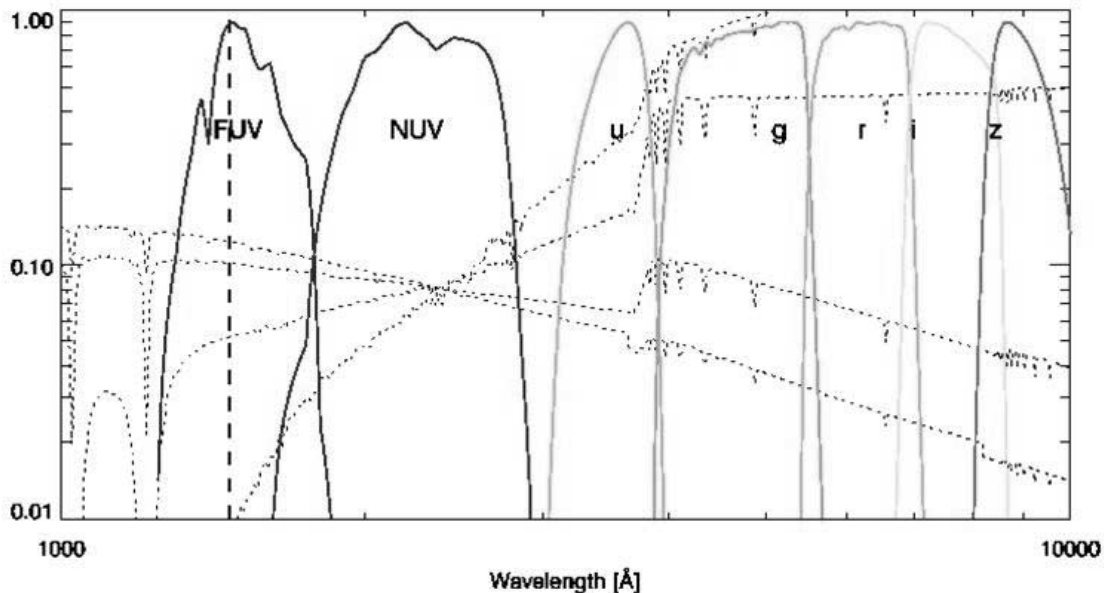
produce representative spectral energy distributions (SEDs) for stars, quasars, and galaxies detected by these two surveys and by the Two Micron All Sky Survey (2MASS).

In the next section we briefly describe the three surveys we use in this work. Section 3 describes the process of matching *GALEX*-SDSS objects and of producing a clean photometric sample of matched objects. It also includes a discussion of *GALEX* objects without SDSS counterparts, as well as an analysis of the repeatability of *GALEX* measurements. Section 4 presents an analysis of the optical properties of unresolved and resolved *GALEX*-SDSS sources, a discussion of the SEDs of a number of interesting classes of sources, and an estimate of the UV contribution to the UV through infrared flux of galaxies. We discuss the significance of our results in § 5 and in particular compare them to those in the recently published Yi et al. (2005) and Rich et al. (2005) studies of star formation in early-type galaxies detected by *GALEX*.

2. OBSERVATIONS

GALEX will eventually map the entire sky at wavelengths between 1344 and 2831 Å in two bands: the near-ultraviolet (NUV; $\lambda_{\mathrm{eff}} = 2271$ Å, $\lambda/\Delta\lambda = 90$) and the far-ultraviolet (FUV; $\lambda_{\mathrm{eff}} = 1528$ Å, $\lambda/\Delta\lambda = 200$). When comparing positions to those of the Tycho-2 catalog (Høg et al. 2000), 80% of *GALEX*-detected stars are found within 1″.5 in the NUV and 2″.8 in the FUV of their expected positions (Morrissey et al. 2005). *GALEX*'s 0.5 m telescope and 1°.2 field of view will also be used to make deep observations (greater than tens of kiloseconds) of individual fields of interest, such as the Lockman Hole and the Chandra Deep Field South. The mission's primary science goals are to observe star-forming galaxies and to track galaxy evolution (Martin et al. 2005). The *GALEX* ERO includes 10 fields, three of which are AIS observations that overlap the SDSS footprint. The AIS fields were observed for 113, 111, and 113 s, respectively, and each covers 1.2 deg^2 (the fields overlap slightly, however, so that the total area on the sky is smaller; see Fig. 2). While for most classes of objects in SDSS the SEDs drop off quickly in the UV, the ERO fields are observed to $n \sim 22$ and $f \sim 22$ (NUV and FUV AB magnitudes, respectively), deep

enough that we expect to find *GALEX* counterparts for a large number of SDSS sources.

SDSS is currently mapping one-quarter of the sky at optical wavelengths. SDSS uses a dedicated 2.5 m telescope at the Apache Point Observatory, New Mexico, to produce homogeneous five-color *u*, *g*, *r*, *i*, *z* CCD images to a depth of $r \sim 22.5$ mag (Fukugita et al. 1996; Gunn et al. 1998; Smith et al. 2002; Hogg et al. 2001) accurate to 0.02 mag (both absolute calibration and rms scatter for sources not limited by photon statistics; Ivezić et al. 2004). Astrometric positions are accurate to better than 0″.1 (rms) in each coordinate for sources with $r < 20.5$ (Pier et al. 2003), and the morphological information from the images allows reliable star-galaxy separation to $r \sim 21.5$ (Lupton et al. 2002). The survey's coverage of $\sim 10^4$ deg^2 in the north Galactic cap and ~ 200 deg^2 in the southern Galactic hemisphere will result in photometric measurements for over 10^8 stars and a similar number of galaxies. In addition, SDSS will obtain spectra for over 10^6 objects, including 10^6 galaxies and 10^5 quasars. The third public data release includes imaging data for 5282 deg^2 of sky and catalogs 1.4×10^8 objects (Abazajian et al. 2005).

Finally, in constructing UV through infrared SEDs for our UV-selected sample of objects, we also use data from 2MASS. This survey used two 1.3 m telescopes to survey the entire sky in near-infrared light.[9] Each telescope's camera was equipped with three 256×256 arrays of HgCdTe detectors with 2″ pixels and observed simultaneously in the J (1.25 μm), H (1.65 μm), and K_s (2.17 μm) bands. The detectors were sensitive to point sources brighter than about 1 mJy at the 10 σ level, corresponding to limiting (Vega-based) magnitudes of 15.8, 15.1, and 14.3 mag, respectively. Point-source photometry is repeatable to better than 10% precision at this level, and the astrometric uncertainty for these sources is less than 0″.2. The 2MASS catalogs contain positional and photometric information for $\sim 5 \times 10^8$ point sources and $\sim 2 \times 10^6$ extended sources. Finlator et al. (2000) and Ivezić et al. (2002) describe the properties of sources detected by both SDSS and 2MASS (in
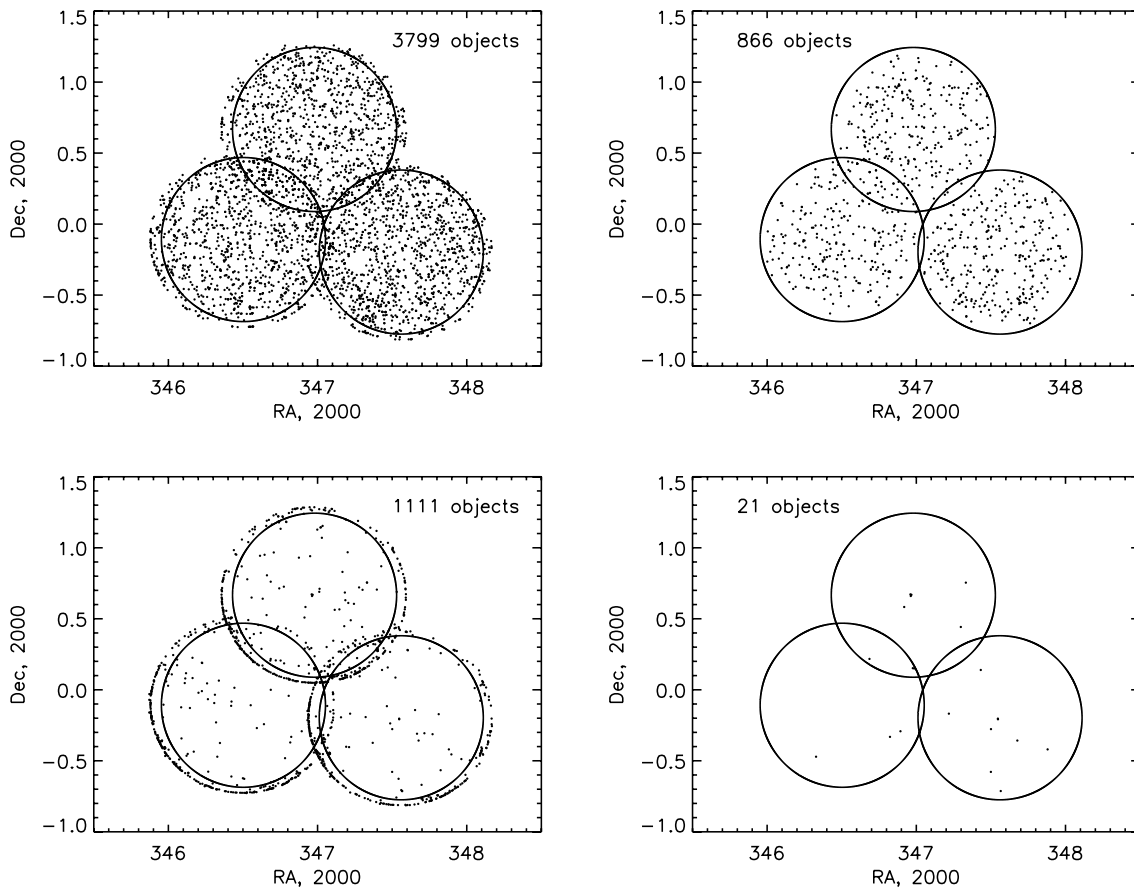
---

[9] See http://www.ipac.caltech.edu/2mass.

FIG. 2.—Distribution of both matched and unmatched *GALEX* sources; matches imply an SDSS source cataloged within 6″ of the *GALEX* position. *Top left*: *GALEX* sources with an SDSS counterpart. *Bottom left*: *GALEX* sources without an SDSS counterpart. *Right*: Distribution with several quality cuts applied to the *GALEX* and SDSS data for matched sources (*top*) and unmatched sources (*bottom*). The circles represent the $R = 0°.55$ field of view for which *GALEX* astrometry is most accurate.

particular, Fig. 3 in Finlator et al. compares the SDSS and 2MASS bandpasses and is analogous to Fig. 1 in this paper).

3. MATCHING *GALEX* AND SDSS

3.1. *Positional Offsets*

The astrometry for both the *GALEX* and SDSS surveys is sufficiently accurate that the typical astrometric errors are much smaller than the average source separation; this significantly simplifies the matching algorithm. We begin by correlating the *GALEX* source positions with positions in the SDSS catalog, taking a 6″ matching radius. This corresponds to the FWHM angular resolution for the NUV channel (Morrissey et al. 2005). Figure 2 illustrates the results of this matching: of the 4910 UV-detected objects in the three *GALEX* fields, we find optical counterparts for 3799 sources (77%), of which 686 (18%) are saturated in the optical. About 5% of matched *GALEX* sources have more than one SDSS counterpart.[10] This is consistent with random matching, based on the mean separation between two SDSS sources of ∼30″. In these cases we simply take the closest match for evaluating sample completeness and limit the matching radius to 3″ when studying colors of matched sources in § 4 (for this matching radius, less than 1% of *GALEX* matches have more than one SDSS counterpart).

A closer look at the matches—and especially the non-matches, those *GALEX* objects without an SDSS counterpart—

shows clear structure in the pattern of matching (see Fig. 2, *bottom left*). Objects along the edges of the *GALEX* field of view are far more likely not to have an optical counterpart. This is mainly due to distortions in the *GALEX* fields and to problems in the flat-fielding along the field edges; as a result, many spurious sources are detected by the *GALEX* data analysis pipeline (T. Wyder 2004, private communication). To avoid this contamination, we select an inclusion distance from the *GALEX* field center of $R \leq 0°.55$, which defines the size of the effective area of each of the three fields overlapping with SDSS. We then have 3007 *GALEX* sources with SDSS counterparts and only 192 without a match within 6″, or 94% and 6%, respectively, of the total number of *GALEX* sources within the area defined above.

Further cuts are then applied to the data to obtain the highest quality sample of *GALEX*-SDSS sources. We determine the *GALEX* faint completeness limit from a histogram of the n magnitudes of *GALEX* sources with an SDSS counterpart and within 0°.55 of their respective field centers (Fig. 3). *GALEX* sources begin to drop out at $n \gtrsim 22$ mag; we select $n = 21.5$ mag as a conservative completeness limit for our sample. For the optical counterparts we require 14 mag $< g <$ 22 mag. Furthermore, we apply a number of conditions based on data-processing flags in the two data sets. We require that the optical counterpart be a unique detection and not saturated in SDSS (for details, see Stoughton et al. 2002). We also require that the *GALEX* artifact flag be set to zero for both the NUV and FUV detections. Bright-star halos appear to be one of the major sources of artifacts in both the NUV and FUV *GALEX* data sets, while other problems

---

[10] Note that this fraction of multiply matched *GALEX* sources is somewhat lower than that reported by Seibert et al. (2005a).
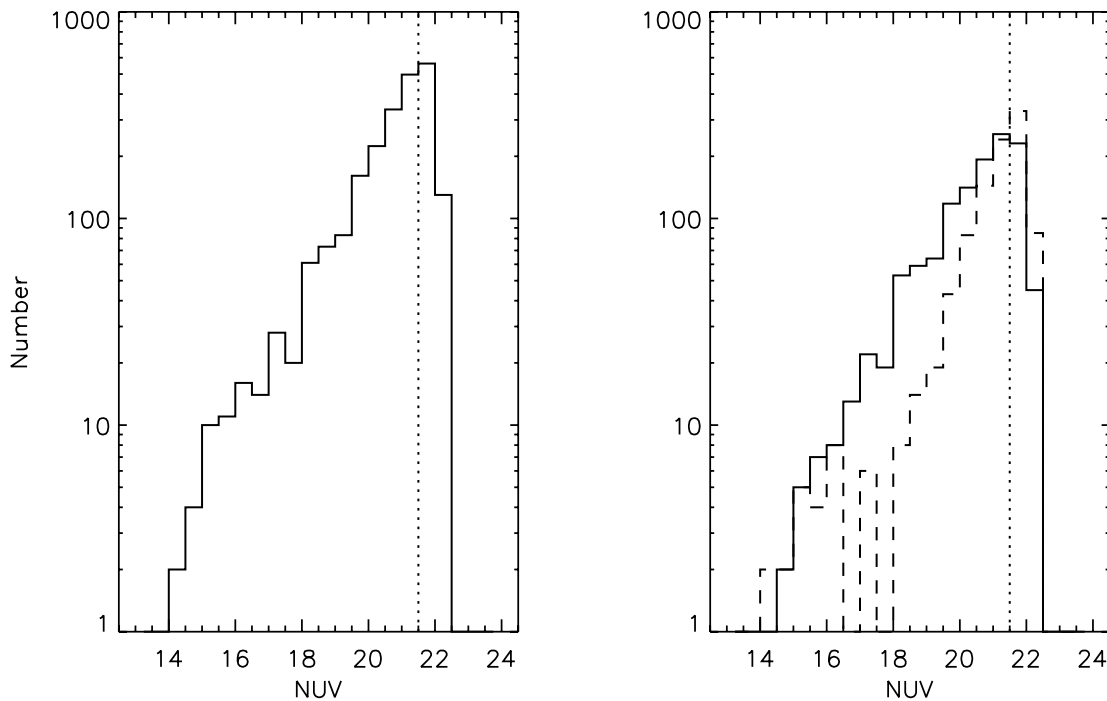
Fig. 3.—*Left*: Differential *n*-magnitude distribution for the unflagged *GALEX* sources with SDSS counterparts. We adopt $n = 21.5$ mag as the *GALEX* faint completeness limit (*dotted line*). *Right*: Separate distributions for the optically unresolved (*solid line*) and resolved (*dashed line*) sources.

(dichroic ghosts or detector hot spots, for example) tend to preferentially affect one set of detections or the other.[11]

The sky distribution of the resulting sample of 866 matched, "clean" sources is shown in Figure 2 (*top right*). Table 1 gives the median astrometric offsets and standard deviations for each

_____

[11] See http://www.galex.caltech.edu/EROWebSite/Early_release_data_description_part3.htm for a full description of *GALEX* image artifacts.

of the three *GALEX* fields and for the overall list of matched sources; for comparison, the offsets obtained during all three of the matching procedures described above are included (i.e., for all matched *GALEX*-SDSS sources, for matches with $R \leq 0°.55$, and for clean matches). Figure 4 illustrates these results.

We note that eliminating matches based on the *GALEX* NUV/ FUV flags strongly impacts the spatial distribution of acceptable matches, so that there now seems to be a dearth of clean sources near the edges of the $R \leq 0°.55$ disks. This suggests that

TABLE 1
POSITIONAL OFFSETS BETWEEN *GALEX* AND SDSS SOURCES

GALEX FIELD CENTER		R.A.$_{GALEX}$ − R.A.$_{SDSS}$ MEDIAN ± σ (arcsec)	Decl.$_{GALEX}$ − Decl.$_{SDSS}$ MEDIAN ± σ (arcsec)
R.A.	Decl.		
All Matches			
23 06 00.72	−00 06 32.4	−0.88 ± 1.95	0.19 ± 1.88
23 07 55.21	+00 39 57.6	−0.44 ± 1.83	−0.10 ± 1.89
23 10 14.64	−00 11 49.2	−0.44 ± 1.90	−0.38 ± 1.86
Combined fields		−0.55 ± 1.90	−0.13 ± 1.88
Matches with $R \leq 0°.55$			
23 06 00.72	−00 06 32.4	−0.99 ± 1.80	0.27 ± 1.74
23 07 55.21	+00 39 57.6	−0.55 ± 1.62	−0.02 ± 1.74
23 10 14.64	−00 11 49.2	−0.55 ± 1.76	−0.32 ± 1.64
Combined fields		−0.66 ± 1.73	−0.07 ± 1.68
Clean Matches			
23 06 00.72	−00 06 32.4	−1.10 ± 1.24	0.24 ± 1.20
23 07 55.21	+00 39 57.6	−0.66 ± 1.30	0.00 ± 1.18
23 10 14.64	−00 11 49.2	−0.55 ± 1.18	−0.31 ± 1.22
Combined fields		−0.66 ± 1.25	−0.06 ± 1.21

NOTE.—Units of right ascension are hours, minutes, and seconds, and units of declination are degrees, arcminutes, and arcseconds.
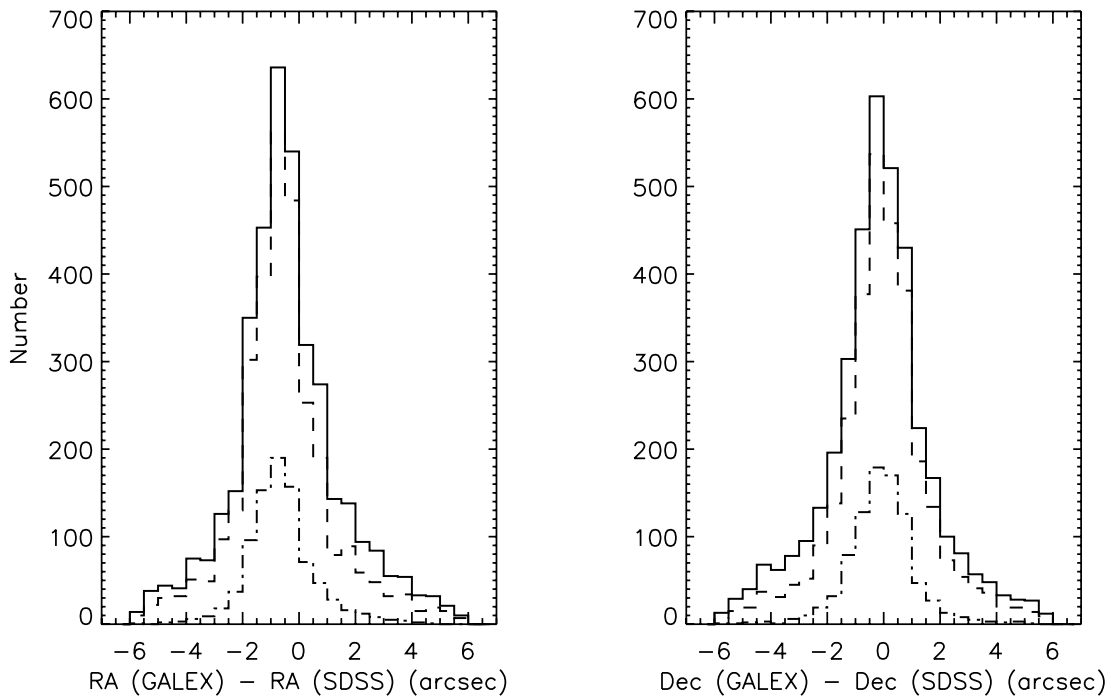
FIG. 4.—Distribution of positional offsets for *GALEX* sources with SDSS counterparts. The solid lines represent all 3799 matches. The dashed lines represent the 3007 matched objects less than 0°.55 from the center of the *GALEX* field, while the dot-dashed lines represent the 866 objects satisfying a number of photometric criteria in both surveys and constituting our cleanest sample of matches. The median values and the rms scatter for these distributions are listed in Table 1.

perhaps the *GALEX* flags are in fact too conservative and that we are losing good matches in these regions.

3.2. *Unmatched GALEX Sources*

Interestingly, it appears that a handful (21) of *GALEX* sources have no SDSS counterparts within 6″, even when highly restrictive quality cuts are applied. These sources are listed in Table 2, and their positions are plotted in Figure 2 (*bottom right*). We used the Multimission Archive at the Space Telescope Science Institute (MAST)[12] and the SDSS Image List Tool[13] to examine the *GALEX* and SDSS "postage stamp" images for all 21 sources (see Figs. 5 and 6 for mosaics of these images).

Extended galaxies.—The only *GALEX* sources without an SDSS counterpart detected both in the NUV and FUV, J230734.52−001731.04 and J230919.65+004515.64, are associated with optically large SDSS galaxies whose centers are farther than 6″ from the *GALEX* position; this large separation explains why they were not matched (for SDSS J230920.2+004523.3, the counterpart to J230919.65+004515.64, a spectrum is available; this is clearly an emission-line galaxy). In addition, J230644.65+001302.13, detected only in the NUV band, also appears to be associated with a galaxy, although here the *GALEX* source is positioned on the very edge of the optically detected galaxy (see Fig. 5, *top right*).

In all these cases the *GALEX* source extraction pipeline (based on SExtractor; Bertin & Arnouts 1996) did not label the sources as artifacts but did set the extraction flag to 3 in all the bands in which it claimed a detection, indicating that the object was originally blended. These detections are supported by the

recent work of Thilker et al. (2005), who observe significant *GALEX* emission at large radii in nearby galaxies. Our off-center detections may be UV emission coming from star-forming regions at large galactic radii, similar to those found in the tidal tails of the merging system known as "the Antennae" (Hibbard et al. 2005).

Artifacts.—Several other sources appear to be close enough to bright stars that they may in fact be artifacts that were not flagged. J230518.70−002816.29, J230751.11+003936.81, and J230959.96−003441.17 were all flagged by SExtractor as either having bright neighbors close enough to bias the photometry (flag = 1) or having originally been blended sources (flag = 2). While J230717.62−001853.40, J230852.36−001005.47, and J231042.50−002126.92 were not flagged at all, their SDSS images suggest that they could indeed be due to bright-star halos (see Fig. 5, *middle and bottom rows*). We note that J230519.28−002741.34 (cataloged in SIMBAD as GSC 05242−00801; m_B = 11.4, m_V = 11.0),[14] the star responsible for the halo detected as J230518.70−002816.29, is very bright in the NUV: $n = 15.09 \pm 0.01$ ($f = 20.38 \pm 0.21$).

An additional eight *GALEX* sources are found between 1′ and 3′ from SDSS-detected stars with $r < 13.5$ (see Fig. 6, *top three rows*; three of these sources were flagged by SExtractor as having originally been blended). There are 1537 *GALEX* sources detected less than 0°.55 from their respective field centers with $n < 21.5$ and no n or f flags. Assuming that the 14 sources described here are stellar artifacts, we can place an upper limit of 1% for the fraction of the photometric *GALEX* sources that are unflagged artifacts.

Unexplained nonmatches.—Four *GALEX* sources do not have a bright star within a few arcminutes (Fig. 6, *bottom two rows*). J231131.21−002510.96 is the only one flagged by

---

TABLE 2

GALEX Objects without an SDSS Counterpart within 6″

GALEX Name	n	f	Flags?	Likely SDSS Counterpart
Galaxies				
J230644.65+001302.13.........	21.43	N/A	NUV = 3	J230645.4+001309.5, $r = 15.94$, $D = 13\farcs5$
J230734.52−001731.04........	20.04	19.64	FUV, NUV = 3	J230734.4−001737.3, $r = 14.87$, $D = 6\farcs5$
J230919.65+004515.64..........	18.20	19.97	FUV, NUV = 3	J230920.2+004523.3, $r = 13.95$, $D = 11\farcs2$
Likely Stellar Artifacts				
J230518.70−002816.29.........	20.06	N/A	NUV = 1	J230519.2−002741.3, $r = 10.86$, $D = 35\farcs8$
J230717.62−001953.40.........	20.74	N/A	None	J230715.31−002008.8, $r = 14.01$, $D = 37\farcs8$
J230751.11+003936.81.........	21.09	N/A	NUV = 2	J230752.1+003858.5, $r = 13.32$, $D = 41\farcs1$
J230852.36−001005.47.........	21.19	N/A	None	J230853.7−000942.1, $r = 9.85$, $D = 30\farcs8$
J230959.96−003441.17.........	21.18	N/A	NUV = 1	J231002.3−003433.1, $r = 11.20$, $D = 36\farcs0$
J231042.50−002126.92.........	21.20	N/A	None	J231041.6−002133.3, $r = 13.11$, $D = 14\farcs9$
Likely Stellar Artifacts?				
J230740.51+003458.86..........	21.23	N/A	None	J230731.4+003538.1, $r = 11.68$, $D = 2\farcm4$
J230750.47+004018.21..........	21.22	N/A	None	J230752.1+003858.5, $r = 13.32$, $D = 1\farcm4$
J230752.10+004008.03..........	21.31	N/A	None	J230752.1+003858.5, $r = 13.32$, $D = 1\farcm2$
J230754.36+000907.62.........	21.00	N/A	NUV = 2	J230800.1+000710, $r = 12.35$, $D = 2\farcm4$
J230756.56+000859.81.........	20.58	N/A	NUV = 2	J230800.1+000710, $r = 12.35$, $D = 2\farcm0$
J230911.58+002631.83..........	20.74	N/A	None	J230923.4+002727.5, $r = 9.56$, $D = 3\farcm1$
J230943.69+000822.11..........	20.94	N/A	None	J230946.4+001041.5, $r = 10.95$, $D = 2\farcm4$
J231015.82−004246.95.........	21.46	N/A	NUV = 2	J231017.9−004123.5, $r = 12.14$, $D = 1\farcm5$
Unexplained				
J231000.10−001636.82.........	20.19	N/A	None	. . .
J231011.21−001211.11	20.90	N/A	None	. . .
J231011.36−001227.72.........	20.76	N/A	None	. . .
J231131.21−002510.96.........	20.77	N/A	NUV = 2	. . .

Note.—For sources with likely counterparts, the SDSS r magnitude is given, along with a separation D.
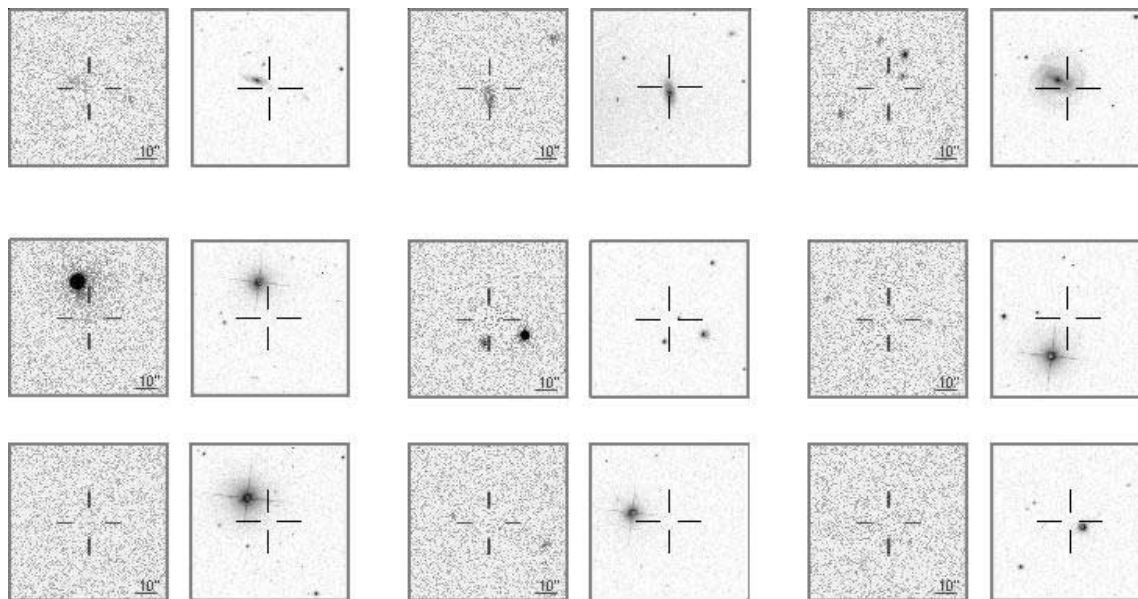

Fig. 5.—NUV-band and composite g, r, i SDSS images of the "explained" unmatched *GALEX* sources (the first nine sources listed in Table 2, *top left to bottom right, reading across the rows*). For each source, the *GALEX* NUV-band image is on the left and the SDSS image is on the right; the images are 150″ on a side with equivalent resolution (the *GALEX* scale bar is 20″, not 10″; S. Salim 2005, private communication). In all the images the crosshairs indicate the quoted position of the *GALEX* source, and north is up and east to the left. The three sources in the top row are most likely associated with the galaxies shown in the optical images. The six sources in the bottom two rows are likely to be missed artifacts—false detections due to nearby bright-star halos. [*See the electronic edition of the Journal for a color version of this figure.*]
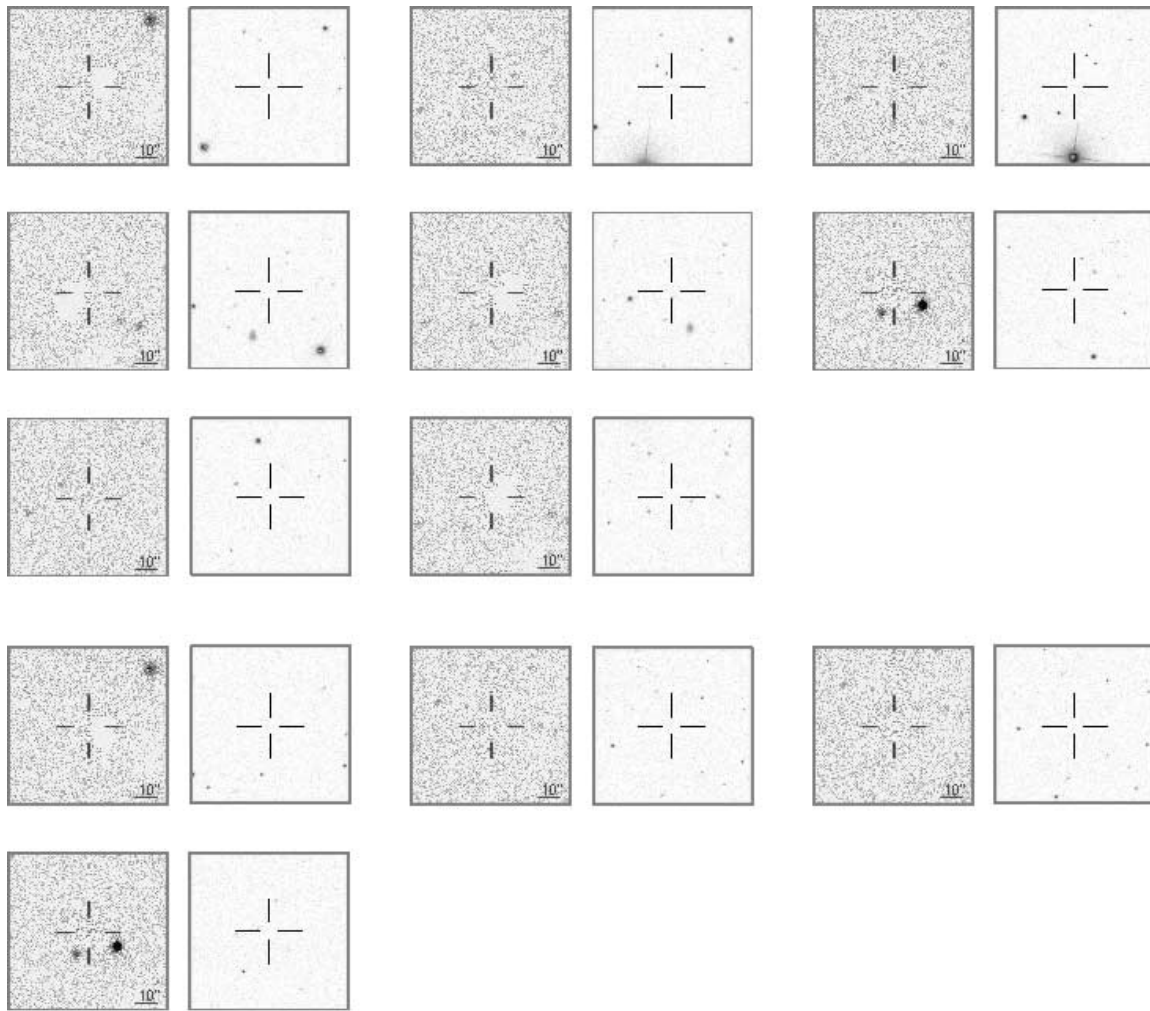
Fig. 6.—NUV-band and composite *g, r, i* SDSS images of the *GALEX* sources (the last 12 sources in Table 2) without SDSS counterparts that are more difficult to interpret. The top three rows show possible stellar artifacts; here, however, the bright star is more than 1′ from the quoted *GALEX* position. As for the four sources whose *GALEX* and SDSS images are shown in the bottom two rows, their nature remains unknown. Only the last one, J231131.21−002510.96, was flagged as suspect by the extraction pipeline. [*See the electronic edition of the Journal for a color version of this figure.*]

SExtractor as having been deblended, suggesting that it is an artifact. However, nothing in MAST provides any explanation for the nature of the other nonmatches. These mysterious sources represent fewer than 0.3% of the total number of photometric *GALEX* sources within 0°55 of the field centers. They do not have counterparts within 30″ cataloged in either SIMBAD or NED,[15] suggesting that they may not be real sources. On the other hand, if their UV detections could be confirmed, they would represent an interesting class of extremely blue (UV-to-optical) sources. A larger sample of *GALEX* sources may indeed provide scores of such objects worthy of further investigation.

In summary, of the 3199 UV sources cataloged with positions within $R \leq 0°55$ of their respective field centers, 192, or 6%, have no SDSS counterpart within 6″. If we make some basic quality cuts on the *GALEX* data, this proportion does not change much: of the 2362 unflagged *GALEX* sources within the 0°55 radius, 130, or 5.5%, are not matched with an SDSS source. Finally, if we require that the sources have $n < 21.5$, there are

1537 *GALEX* sources within the 0°55 radius and only 21, or 1.4%, without an SDSS counterpart.

We can discount 10 of these 21 sources as probable artifacts based on their extraction flags. That leaves 11 UV sources out of 1537, or 0.7%, as photometric *GALEX* sources without an SDSS counterpart within 6″. We have examined the *GALEX* and SDSS images for all 21 of the sources without a counterpart; in a handful of cases, we are unable to identify even an unlikely source (i.e., a distant star's halo) as responsible for the *GALEX* detection. While these comprise fewer than 0.3% of the photometric *GALEX* sources and are likely to be artifacts, they might be objects detected only in the UV and therefore of great interest.

3.3. *The Repeatability of GALEX Measurements*

The three *GALEX* AIS ERO fields overlap slightly. We therefore match the *GALEX* catalogs for the AIS fields with each other in order to characterize the differences between the measurements of objects observed twice. There are 31 multiply observed *GALEX* sources that pass the quality cuts discussed above.

The systematic astrometric offsets in both coordinates are consistent with *GALEX* astrometric errors inferred from comparison with SDSS astrometry. The rms scatter is somewhat

---

[15] This research has made use of the NASA/IPAC Extragalactic Database (NED), which is operated by the Jet Propulsion Laboratory, California Institute of Technology, under contract with the National Aeronautics and Space Administration.

larger (2″), probably because the multiply observed *GALEX* objects are detected near the edges of the fields.

The rms scatter for the *n*-band measurements is 0.33 mag. (Only a small fraction of sources is detected in both bands both times.) The magnitude differences depend on the mean *n* magnitude for $n > 20$. For sources at the bright end (eight sources with $n < 20$) we find that the median offset is 0.13 mag, with an rms of only 0.07 mag. The magnitude difference normalized by the expected error has an rms scatter of 1.4 and, at the bright end, 1.9. This demonstrates that the photometric errors are computed fairly accurately by the *GALEX* photometric pipeline and that systematic errors at the bright end are not very large.

4. ANALYSIS

In this section we first compare the optical properties of matched sources to the full SDSS sample and then extend our analysis by combining UV, optical, and infrared data from *GALEX*, SDSS, and 2MASS. The sample of matched sources analyzed here is UV-selected, since practically every *GALEX* source is detected by SDSS, while only 2.5% of SDSS sources are detected by *GALEX*. Not all *GALEX*-SDSS sources are detected by 2MASS (this is especially true for resolved sources; see Ivezić et al. 2002), but this has no impact on the UV through infrared SEDs discussed in § 4.3.

SDSS color-magnitude and color-color diagrams are a powerful tool to classify detected sources (e.g., Fan 1999; Finlator et al. 2000; Richards et al. 2002; and references therein), thanks to accurate five-band photometry and robust star-galaxy separation. Thus, when studying a subsample of sources selected by other means, such as detections at nonoptical wavelengths, it is very informative to examine their distribution in these diagrams.

The contours in Figure 7 (*top*) outline the distribution of optically unresolved (*left*) and resolved (*right*) SDSS sources in the *r* versus $g - r$ color-magnitude diagram (we use the SDSS model magnitudes; for details, see Stoughton et al. 2002). The matched *GALEX*-SDSS sources are shown by circles (unresolved sources) and squares (resolved sources). For *GALEX* detections we require $n < 21$ or $f < 21$ and correct magnitudes for interstellar extinction using $A_f = 2.97A_r$ and $A_n = 3.23A_r$, where A_r is the *r*-band extinction from the maps of Schlegel et al. (1998), distributed with the SDSS data. These coefficients were evaluated using the standard interstellar extinction law[16] from Cardelli et al. (1989; M. Seibert 2004, private communication). The median A_r for the three AIS fields is 0.12, with an rms scatter of 0.02 mag.

In the remaining panels of Figure 7 SDSS sources (optically unresolved, *dots*; resolved, *contours*) and *GALEX*-SDSS sources (*symbols*) are shown in the $g - r$ versus $u - g$ (*middle*) and $r - i$ versus $g - r$ (*bottom*) color-color diagrams. We discuss these diagrams in the next two sections.

4.1. Unresolved SDSS Sources

The optically unresolved *GALEX*-SDSS sources are dominated by blue turnoff stars ($0.8 < u - g < 1.5$ and $0.2 < g - r < 0.6$; see Fig. 7, *middle left*). The sample also contains low-redshift quasars ($z < 2.2$) and hot white dwarfs (both are identified by their blue $u - g$ colors, $u - g < 0.6$), as well as white dwarf–M dwarf pairs (scattered above the locus; for details, see Smolčić et al. 2004; Pourbaix et al. 2004). The well-defined red

edge of the turnoff star distribution in the *r* versus $g - r$ color-magnitude diagram (at $g - r \sim 0.6$ for $r \sim 14$ and $g - r \sim 0.2$ for $r \sim 19$) is a consequence of the *GALEX* faint limit and the steep dependence of the UV-optical color on the effective temperature (the latter essentially controls the $g - r$ color). For these stars we find that $n - r = f(g - r) = 12.3(g - r) - 0.47$, and thus the faint limit in the *GALEX* n band ($n < 21$) defines the observed red edge: $r < 21.47 - 12.3(g - r)$.

Figure 8 (*top left*) shows the distribution of optically unresolved *GALEX*-SDSS sources in the *n* versus $n - u$ color-magnitude diagram. Sources detected only in the *GALEX* NUV band are shown as small dots, and those with detections in both the FUV and NUV bands are shown as large dots. The easily discernible bimodal distribution of the $n - u$ color is well correlated with the distribution of the SDSS $u - g$ color, as shown in Figure 8 (*top right*). The boundary $n - u = 1.3$ corresponds to $u - g = 0.6$, which separates turnoff stars from hotter stars ($T_{\mathrm{eff}} > 10,000$ K) and low-redshift quasars. The last two classes dominate the optically unresolved sources detected in both *GALEX* bands. As discernible from Figure 8 (*middle left*), the fraction of *GALEX*-SDSS sources detected in both *GALEX* bands is much higher for hot stars ($u - g < 0.6$, $g - r < -0.2$, dominated by white dwarfs) than for quasars ($u - g < 0.6$, $g - r > -0.2$). This is a consequence of the *GALEX* faint limit in the FUV band and the fact that the $f - n$ color is *bluer* for hot stars than for quasars (see Fig. 8, *middle right*). In addition, quasars at redshifts beyond ~ 0.5 may be very faint in the *f* band because the Lyα line is redshifted to the *n* band.

4.2. Resolved SDSS Sources

The optically resolved *GALEX*-SDSS sources are dominated by galaxies *fainter* than the SDSS spectroscopic limit for the main sample ($r_{\mathrm{Pet}} = 17.8$)[17] but mostly brighter than $r = 21$, as discernible from Figure 7 (*top right*). *GALEX*-SDSS galaxies are predominantly blue ($0.2 < g - r < 0.8$, or $u - r < 2.2$; for a discussion of the bimodal $u - r$ color distribution of galaxies, see Strateva et al. 2001), while a small fraction have colors consistent with those of active galactic nuclei (AGNs) ($2 < u - r < 3$; M. Obrić et al. 2005, in preparation).

The distribution of optically resolved *GALEX*-SDSS sources in the *n* versus $n - u$ color-magnitude diagram is shown in Figure 8 (*bottom left*), where those detected only in the *GALEX* NUV band are shown as small dots, and those with detections in both the FUV and NUV bands are shown as large dots. Unlike optically unresolved sources, whose detection in both *GALEX* bands is strongly correlated with the $n - u$ color, the fraction of optically resolved sources detected in both *GALEX* bands is strongly correlated with brightness: galaxies brighter than $n = 20.5$ typically have both detections, and those with only one detection are dominated by galaxies with $n > 20.5$. The fairly narrow $n - u$ color distribution suggests that the mismatching of SDSS and *GALEX* detections and other problems, such as the shredding of extended galaxies by the *GALEX* photometric pipeline discussed by Seibert et al. (2005a), are not significant for this sample.

Galaxies that have undergone recent starbursts have UV fluxes dominated by their most massive young stars. These hot stars have $T_{\mathrm{eff}} > 10,000$ K and UV spectral slopes ($f - n$ colors) similar to those of hot white dwarfs. As these galaxies

---

[16] The standard Milky Way extinction curve predicts that the $f - n$ color becomes *bluer* with increasing extinction; this is a consequence of the strong feature at 0.22 μm (e.g., Fig. 21 in Calzetti et al. 1994).

[17] The SDSS Petrosian magnitude, r_{Pet}, is computed using the Petrosian flux. The Petrosian flux is measured in a circular aperture of radius twice the Petrosian radius, where the latter is defined by the ratio of the averaged and local surface brightness. See Strauss et al. (2002) for details.
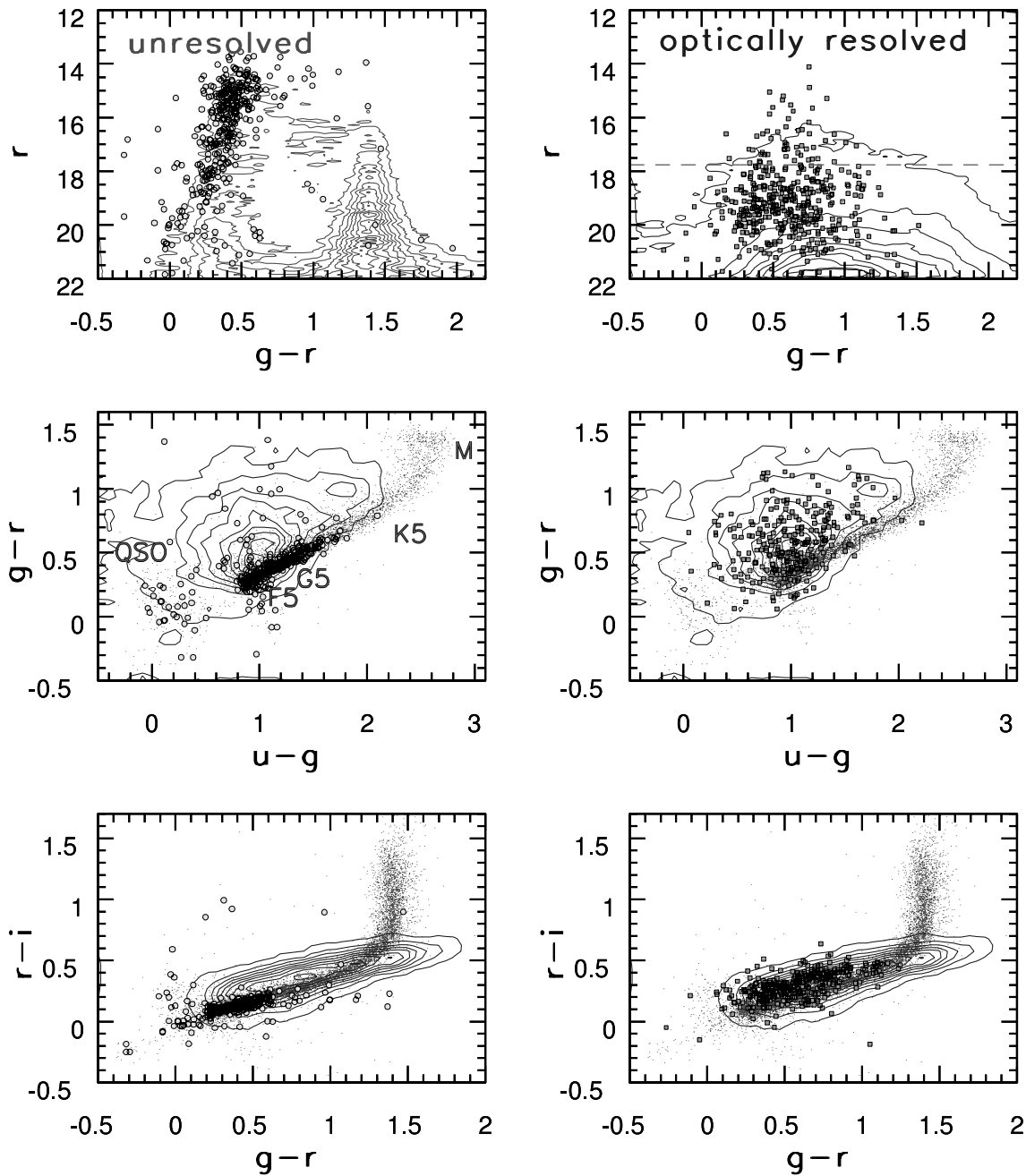
FIG. 7.—*Top*: Comparison of distribution of SDSS sources detected by *GALEX* (*symbols*) to the overall distribution of all SDSS sources in the *r* vs. *g − r* color-magnitude diagrams for one of the three *GALEX* AIS ERO fields discussed here. The left panel shows optically unresolved sources, and the right panel shows optically resolved sources. The dashed line (*top right*) indicates the faint flux limit for the SDSS spectroscopic main sample ($r_{Pet} < 17.8$). *Middle and bottom*: Color-color diagrams in which the distributions of all SDSS unresolved sources are shown by dots, and those for galaxies are shown by contours (*same for both left and right panels*). The *GALEX*-SDSS sources are marked by large symbols (unresolved [*left*] and resolved [*right*]). The approximate positions of low-redshift quasars and a few characteristic stellar spectral types are shown (*middle left*). [*See the electronic edition of the Journal for a color version of this figure.*]

age, stellar evolution will preferentially remove the hottest, bluest members first, and their UV color will grow redder.[18] By comparison, the UV flux of AGN host galaxies is dominated by emission from their central source, whose UV spectral slope is similar to that of (unresolved) low-redshift quasars.

In Figure 8 (*middle right*) we divide the $g − r$ versus $f − n$ color-color diagram for unresolved sources into regions dominated by hot white dwarfs ($f − n < 0$, $g − r < −0.2$) and low-redshift quasars ($f − n > 0$, $g − r > −0.2$). *GALEX* pho-

tometric errors should make negligible contributions to the observed color dispersion, as our flux limits are conservative ($n < 21$ and $f < 21$); nevertheless, some of the extreme color outliers could reflect non-Gaussian errors, such as the pipeline's treatment of complex or blended sources or *GALEX*-SDSS mismatches. In addition, dust attenuation may affect the integrated $f − n$ color of galaxies and bias the implied stellar ages discussed below toward larger values. Using the model results from Salim et al. (2005), we estimate that the median reddening of the $f − n$ color due to dust may be about 0.5 mag. For this reason, we emphasize that the adopted $f − n = 0$ boundary is intrinsically fuzzy.

---

[18] According to models by Bianchi et al. (2005), the $f − n$ color changes from −0.35 to −0.06 to 0.18 as a single stellar population ages from 1 to 10 to 100 Myr.
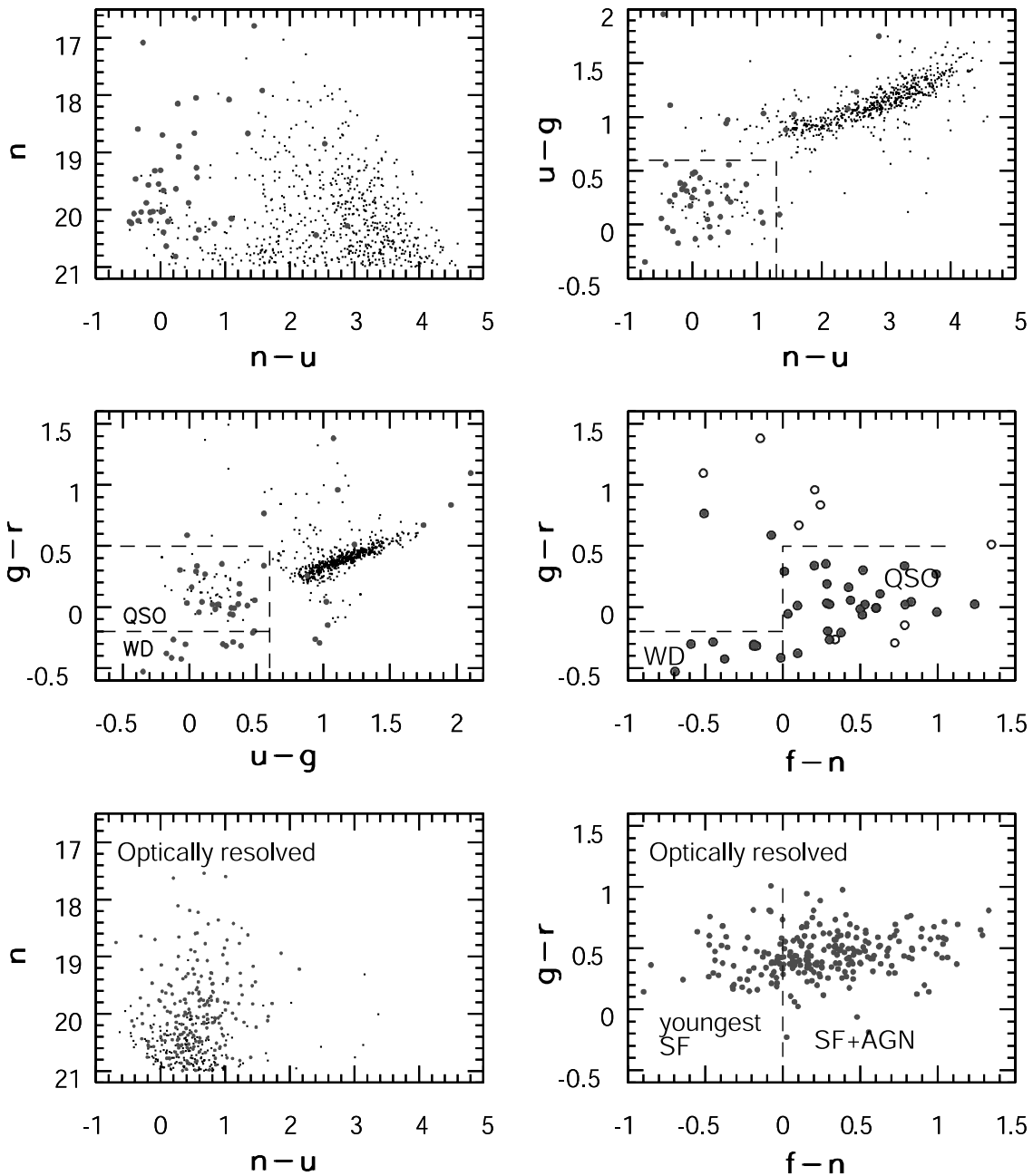
Fig. 8.—*GALEX*-SDSS UV-optical color-color and color-magnitude diagrams for all sources from the three *GALEX* AIS ERO fields discussed here. *Top and middle*, optically unresolved sources; *bottom*, galaxies. The small dots represent sources detected only in the *GALEX n* band, and the large dots represent those detected in both *GALEX* bands. In the middle right panel, open circles indicate objects with $u - g > 0.6$, and filled circles indicate objects with $u - g < 0.6$ (among the latter, white dwarfs dominate for $g - r < -0.2$ and low-redshift quasars for $g - r > -0.2$); note that white dwarfs (WD) have bluer $f - n$ colors than quasars (QSO). The dashed line (*bottom right*) separates galaxies with the youngest starbursts (*left of line*) from those consistent both with intermediate-age starbursts and with AGN emission (*right of line*), as inferred from comparison with the middle right panel. [*See the electronic edition of the Journal for a color version of this figure.*]

As shown in Figure 8 (*bottom right*), comparing the colors of *GALEX*-SDSS galaxies to those of the unresolved sources suggests that *GALEX*-SDSS galaxies with $f - n < 0$ are likely to be the youngest starburst galaxies, with UV colors still dominated by flux from very hot stars. (Plausible ages, inferred from models, are less than ~20 Myr; e.g., Bianchi et al. 2005.) Furthermore, this sample should not suffer seriously from AGN contamination, as relatively few low-redshift quasars have $f - n$ colors this blue.

Resolved sources with $f - n > 0$, however, while consistent with a population of older starburst galaxies, may also contain a significant fraction of AGN hosts, given that low-redshift quasars share this UV color space. While *GALEX* $f - n$ colors

will provide constraints on the star formation history with greater precision than is possible from SDSS data, since the *GALEX* $f - n$ color varies substantially more than the SDSS $g - r$ color [$\Delta(f - n)/\Delta(g - r) \sim 4$], additional information, such as spatially resolved FUV emission or X-ray and radio data, is needed before the *GALEX* UV color can be unambiguously interpreted as a sign of recent star formation. An analogous conclusion follows from the distribution of the $n - u$ color: for the majority of *GALEX*-SDSS galaxies, $n - u$ is bluer than the $n - u$ color for turnoff stars in the galaxy and is similar to $n - u$ colors of *both* quasars and hot stars (compare the top left and bottom left panels in Fig. 8).
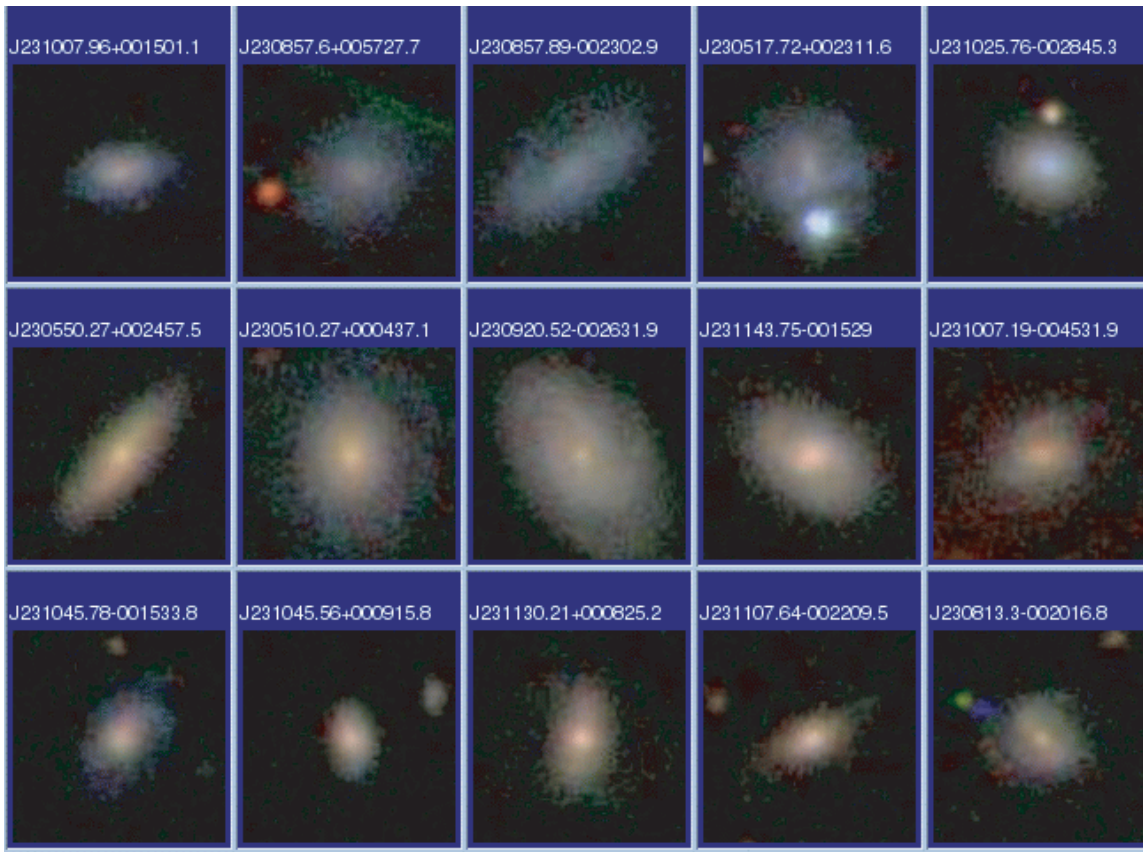
Fig. 9.—Composite g, r, i SDSS images of a randomly chosen sample of main galaxies detected by *GALEX* from among those discussed and classified by M. Obrić et al. (2005, in preparation). Images are of star-forming galaxies (*top*), AGNs (*middle*), and galaxies with uncertain classifications based on their emission-line ratios (*bottom*). North is up, and the images are roughly 25″ on a side.

Further evidence that a blue UV color for *GALEX*-SDSS galaxies does not necessarily imply starburst emission comes from a detailed analysis of emission-line strengths measured from SDSS spectra. M. Obrić et al. (2005, in preparation) study the multiwavelength properties of SDSS main spectroscopic galaxies and find that about 40% of them are detected by *GALEX*. Of those, 70% are emission-line galaxies, which they classify as AGNs, star-forming, or "inconclusive" using line strength ratios. They find that *at least 10% of SDSS main galaxies detected by GALEX have emission lines indicating an AGN, with the true fraction possibly as high as 30%.* We have visually inspected SDSS g, r, i color composite images of these galaxies (a total of 55) and found that the classification based on emission-line strengths is well correlated with morphology. SDSS images of a random subsample of M. Obrić et al. *GALEX*-SDSS AGNs, star-forming galaxies, and inconclusive galaxies are presented in Figure 9 and show clear morphological differences between galaxies classified as star-forming and those classified as AGNs, with the latter being more centrally concentrated. These morphological differences further demonstrate that at least some *GALEX*-SDSS galaxies are more likely to be AGNs than star-forming. In Table 3 we list M. Obrić et al.'s measurements of the light concentration indices (see Strateva et al. [2001] for details) and emission-line strengths, SDSS redshifts, and *GALEX*, SDSS, and 2MASS photometry and colors for the AGN candidates in Figure 9. We note that one of the AGN candidates, SDSS J230920.52−002631.9, is cataloged by SIMBAD as the Seyfert 1 galaxy [VV2003c] J230920.5−002632, while another, SDSS J231143.75−001529, is <1″ from a cataloged FIRST source (Becker et al. 1995).

Finally, we note that although young stellar populations dominate the UV flux from starburst galaxies, their contribution to the UV through infrared flux is very small, as inferred from the red $g − r$ colors for these sources ($g − r \sim 0.3$, unlike the $g − r \sim −0.4$ typical for stars with $f − n < 0$). We further discuss the contribution of UV light to the UV through infrared flux below.

4.3. *The 10-Band UV through Infrared Spectral Energy Distributions*

In addition to color-color and color-magnitude diagrams, an efficient way to analyze data that span such a wide wavelength range is to construct the SEDs for various classes of sources. Here we analyze the turnoff stars, hot stars, low-redshift quasars, and two subsamples of galaxies. We expand the wavelength range by including 2MASS data, and we use the Vega-to-AB conversion for 2MASS magnitudes as described by Finlator et al. (2000): $J_{AB} = J_{2MASS} + 0.89$, $H_{AB} = H_{2MASS} + 1.37$, $K_{AB} = K_{2MASS} + 1.84$. The SEDs are presented in the $\lambda F_\lambda (= \nu F_\nu)$ form, normalized to 1 at 2.2 μm (2MASS K_s band).

For hot and turnoff stars, we select subsamples in the SDSS $g − r$ versus $u − g$ color-color diagram (see § 4.1 and Fig. 7) and use the median colors (e.g., for $f − n, n − u, \ldots, H − K_s$) to construct their SEDs. Optical colors of low-redshift quasars vary by a few tenths of a magnitude as a function of redshift because of emission-line effects (Richards et al. 2001). We adopt optical colors representative of objects at $z = 1$ (i.e., roughly the median redshift). The sample of *GALEX*-SDSS low-redshift quasars discussed here is not sufficiently large to constrain the dependence of UV colors on redshift, and we

TABLE 3
Characteristics of the Five *GALEX*-SDSS AGNs Presented in Figure 9

Parameter	J230550.27+002457.5	J230510.27+000437.1	J230920.52−002631.9	J231143.75−001529	J231007.19−004531.9
R.A. (deg)	346.459	346.293	347.336	347.932	347.530
Decl. (deg)	0.416	0.077	−0.442	−0.258	−0.759
CI[a]	2.40	2.68	2.03	2.40	2.18
[N II]/H$_\alpha$[a]	−0.19	−0.32	−0.13	−0.16	0.06
[O III]/H$_\beta$[a]	−0.08	−0.11	0.56	0.48	−0.23
z	0.062	0.056	0.035	0.060	0.111
$f - n$	−0.08	0.48	0.54	0.73	1.28[b]
n	20.23	18.36	18.77	18.71	18.64
$u - g$	1.59	1.47	1.39	1.28	4.01
$g - r$	0.80	0.67	0.62	0.64	0.81
$r - i$	0.42	0.37	0.32	0.37	0.34
$i - z$	0.30	0.24	0.23	0.22	0.37
r	16.37	15.34	15.53	15.76	17.53
A_r	0.12	0.14	0.10	0.13	0.10
$J - K_s$	1.10	1.11	1.05	1.00	1.06
J	15.53	15.59	16.00	14.85	16.13
H	14.88	14.89	14.11[c]	14.21	15.54
Comments	...	LEDA 1156491	Seyfert 1	FIRST source	...

[a] Measurements of light concentration indices (CI) and emission-line strengths from M. Obrić et al. (2005, in preparation).
[b] A nearby $r = 10$ star (saturated in SDSS) is likely to have affected the *GALEX* n and SDSS u measurements.
[c] Upper limit.

simply adopt the median values for $f - n$ and $n - u$ colors. For 2MASS colors (which vary less as a function of redshift than do the optical colors), we take the median values of $z - J$, $J - H$, and $H - K_s$ colors for a sample of low-redshift quasars discussed by K. R. Covey et al. (2005, in preparation; these values agree well with the results of Finlator et al. 2000). The SEDs for these three representative classes of optically unresolved sources are shown in Figure 10 (*top*). Note that the well-known 1 μm inflection in the quasar SED (e.g., Elvis et al. 1994) is properly reproduced.

The observed broadband colors of a galaxy depend on both its type and its redshift (*K*-correction). Because of the limited redshift range of the galaxies discussed here, the observed color dispersion is dominated by the difference in galaxy type. Following Strateva et al. (2001), we separate galaxies in two dominant subsamples using the SDSS $u - r$ color; in practice, this roughly corresponds to a morphological division into spiral and elliptical galaxies. The effect of *K*-correction on measured optical and infrared galaxy colors is discussed in detail by M. Obrić et al. (2005, in preparation). Of the 99,000 main galaxies they study, 1880 blue and 3400 red galaxies listed in the 2MASS Extended Source Catalog and selected from the narrow redshift range $0.03 < z < 0.05$ are used to construct these SEDs. For the $u - r < 2.2$ subsample we adopt the median $f - n$ and $n - u$ colors for the *GALEX*-SDSS galaxies discussed here. For the $u - r > 2.2$ subsample only the $n - u$ median color is used, while for the $f - n$ color we adopt a lower limit, based on the color of the *GALEX* faint flux limits. (Most of those galaxies are not detected in the f band.) The SEDs for the two dominant types of galaxies are shown in Figure 10 (*bottom*). The error bars indicate the rms scatter in each color and for each subsample.

The comparison of the UV parts of SEDs for optically unresolved sources and galaxies further illustrates the conclusions from the preceding section. The very blue UV color for galaxies detected in both *GALEX* bands cannot be due to stars with ages similar to those of the turnoff stars from the Galaxy. On the other hand, the observed UV slope is consistent with the UV slope for both hot stars and low-redshift quasars. The contribution of the UV flux to the UV through infrared flux of galaxies is discussed next.

4.4. *The UV Contribution to the UV through Infrared Flux of Galaxies*

M. Obrić et al. (2005, in preparation) present an analysis of the dependence of galaxy SEDs on galaxy type. For each dominant galaxy type (defined by the $u - r$ color division of Strateva et al. 2001) they compute the integrated flux in the 0.2–2.2 μm range covered by *GALEX*, SDSS, and 2MASS data. Although we hereafter refer to this flux as the bolometric flux, note that it does not include the contributions from wavelengths longer than 2.2 μm, which, for galaxies with strong mid- and far-infrared emission, could be as large as, or larger than, those from the 0.2–2.2 μm region. (The contributions from wavelengths shorter than 0.2 μm are most likely not important.) M. Obrić et al. demonstrate that galaxy SEDs, when normalized by this bolometric flux, cross at a wavelength corresponding to the SDSS z band, regardless of the galaxy type. In other words, the bolometric correction for galaxies in the z band is independent of type, and thus the z-band flux and absolute magnitude measurements are good proxies, to within a type-independent constant [which they report as $(\lambda F_\lambda)_z = 0.58 F_{bol}$], for bolometric flux and bolometric luminosity. Hence, the $f - z$ color is a good choice for studying the UV contribution to the bolometric flux of galaxies.

Figure 11 (*top*) shows the $f - z$ color of galaxies detected in both *GALEX* bands as a function of the $f - n$ color. A good degree of correlation is evident; galaxies with the bluest $f - n$ colors also tend to have the bluest $f - z$ colors. The selection effects for the sample shown in Figure 11 are simple and defined by the *GALEX* faint flux limits, since essentially all *GALEX* sources are detected by SDSS. Hence, the correlation between the $f - z$ and $f - n$ colors is an astrophysical relation, rather than, for example, a consequence of missing sources in the top left and bottom right corners due to faint flux limits (for a counterexample, see below). In other words, it is fair to use the
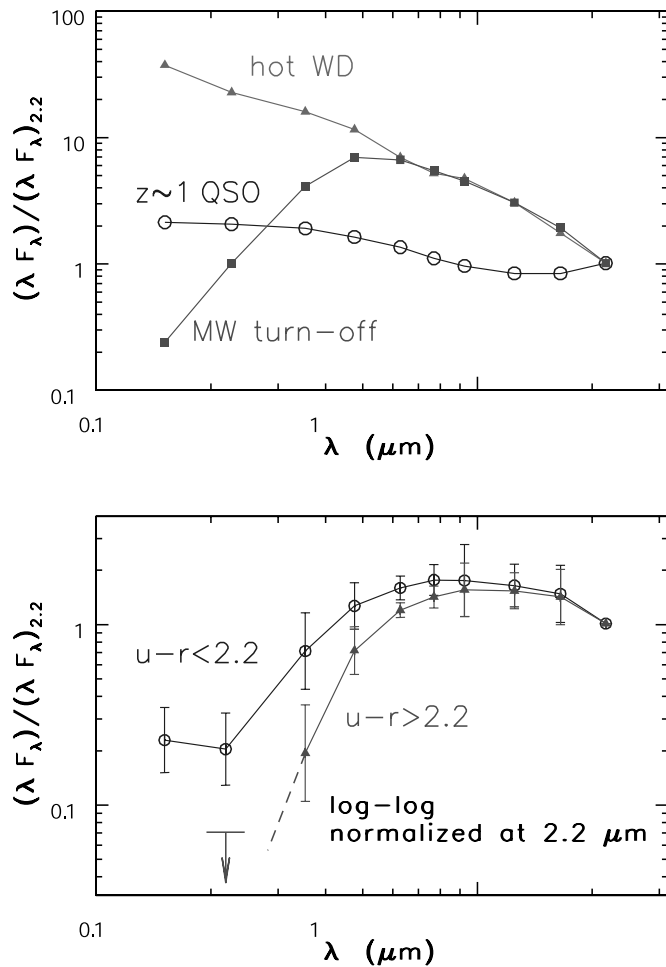
Fig. 10.—*Top*: Median UV-infrared SEDs for low-redshift ($z \sim 1$) quasars (*circles*), hot white dwarfs (*triangles*), and turnoff stars (*squares*) constructed using *GALEX*, SDSS, and 2MASS data (the data points are connected to guide the eye). *Bottom*: Mean SEDs for blue ($u - r < 2.22$; *circles*) and red ($u - r > 2.22$; *triangles*) galaxies, with redshifts in the range $0.03–0.05$. The error bars show the rms color scatter for each subsample, determined from the interquartile range. [*See the electronic edition of the Journal for a color version of this figure.*]

GALEX f and n measurements to predict the SDSS z magnitude. The relation $z = f - 1.36(f - n) - 2.25$, shown by the dashed line in Figure 11 (*top*), predicts unbiased SDSS z-band magnitudes with an rms scatter of only 0.7 mag (see Fig. 11, *middle*).

This correlation probably includes both the effects of the age distribution of stellar populations and dust attenuation effects. If the contribution of dust attenuation is not dominant,[19] then the hottest, and thus youngest, stellar populations seem to have a fair degree of knowledge about the older populations. A detailed study of this interesting possibility, including disentangling the contributions of stellar age and dust attenuation effects, and the transformation to more physical quantities like the current and integrated star formation rate, is beyond the scope of this work and will be addressed elsewhere.

As an example of an apparent correlation between colors due to selection effects, we show the $f - z$ color as a function of the
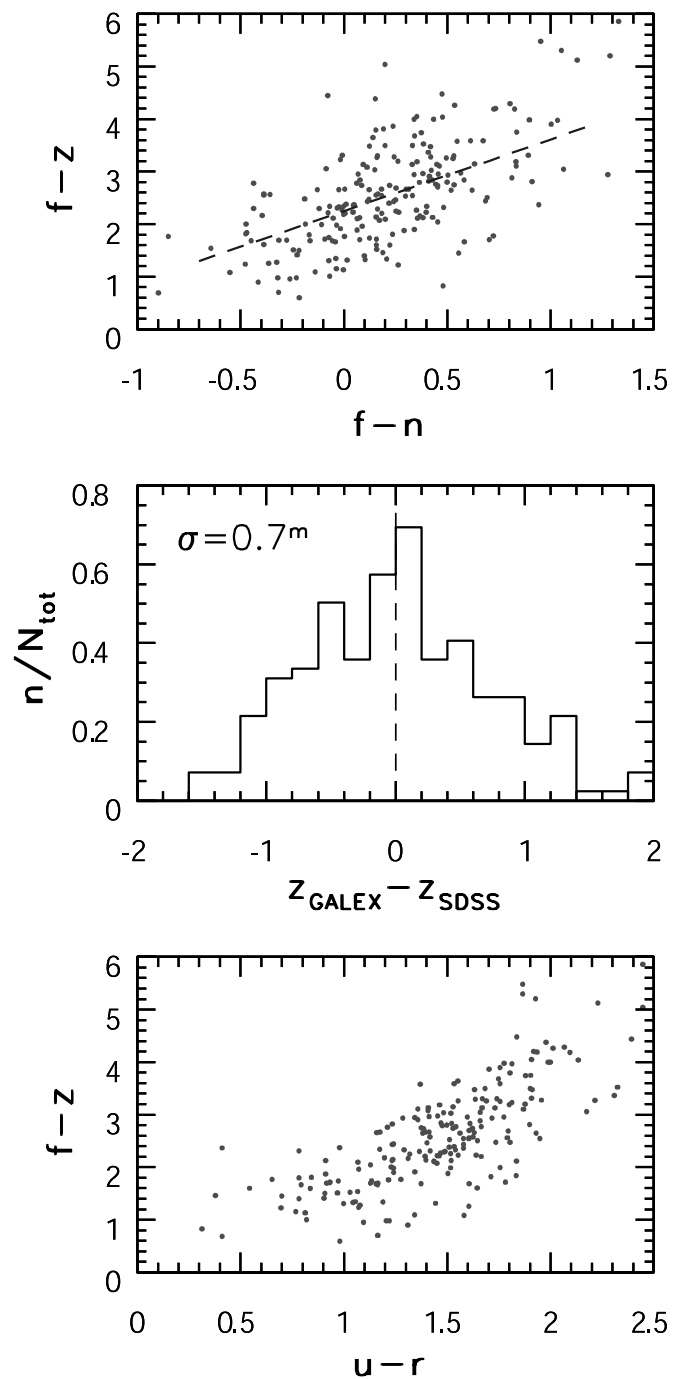

Fig. 11.—*Top*: Correlation between the $f - z$ (UV-infrared color, a measure of the UV contribution to the UV through infrared flux) and $f - n$ (UV slope) colors for galaxies detected in both *GALEX* bands. The dashed line represents a best linear fit $f - z = 1.36(f - n) + 2.25$ to the median $f - z$ color in bins of $f - n$. *Middle*: Distribution of differences between synthetic *GALEX*-based z-band magnitudes computed using this relation and the SDSS-measured z-band magnitudes. *Bottom*: Apparently similar correlation between the $u - r$ and $f - z$ colors. However, this correlation is a consequence of the strong selection effect introduced by the *GALEX* faint flux limit in the f band. [*See the electronic edition of the Journal for a color version of this figure.*]

$u - r$ color in Figure 11 (*bottom*). The distribution of galaxies in this diagram represents a bivariate distribution of the UV contribution to the UV through infrared flux (or luminosity) as a function of the morphological type (i.e., the $u - r$ color). However, *only* those galaxies with substantial UV flux relative to the UV through infrared flux are sufficiently bright to be

---

[19] According to the effective extinction law from Calzetti et al. (1994), $\Delta(f - z)/\Delta(f - n) = 4.1$. Hence, even if that extinction law does not apply exactly (e.g., if the dust is different or if there are unaccounted-for radiative transfer effects), the slope of the observed $f - z$ vs. $f - n$ correlation (1.36) appears too small to be explained only by dust attenuation.

detected by *GALEX*. The sharp $f - z$ cutoff in the distribution of sources running from the bottom left to the top right corner of the panel is therefore a direct consequence of the *GALEX* faint flux limit and does not represent an intrinsic astrophysical correlation. This asymmetry with respect to the $f - z$ versus $f - n$ diagram discussed above comes from the fact that *every* *GALEX* galaxy is detected by SDSS but only *some* SDSS galaxies (those with substantial star formation or perhaps with AGN activity) are detected by *GALEX*. Equivalently, the $f - z$ measurement is available for every galaxy with the $f - n$ measurement but not for every galaxy with the $u - r$ measurement.

In the same way that SDSS z-band magnitudes can be predicted from *GALEX* f and n measurements, the $f - z$ versus $u - r$ correlation can be used to formally predict the f-band flux from the SDSS u-, r-, and z-band measurements with an rms scatter of only 0.6 mag. However, this scatter is simply a measure of the slope of the differential f-magnitude distribution, just above the f-band faint cutoff. With several magnitudes deeper UV data, the apparent correlation in Figure 11 (*bottom*) should disappear, and this scatter should increase considerably.

5. DISCUSSION

This study, despite the relatively small sample of matched objects, indicates the enormous potential of modern, massive, sensitive large-scale surveys and emphasizes the added value obtained by combining data from different wavelengths. The comparison of *GALEX* and SDSS data, as well as the analysis of repeated *GALEX* observations, demonstrates the high quality of the *GALEX* catalogs. We find no significant population of sources detected only by *GALEX*; the ∼1% of *GALEX* sources without a probable SDSS counterpart appears to be dominated by processing artifacts. While the astrometric calibration seems to show systematic offsets of order 1″, the reported photometric errors describe the behavior of *GALEX* photometry quite well.

Although only 2.5% of SDSS sources are detected by *GALEX*, the UV data carry important astrophysical information. For example, the *GALEX* measurements of the UV color allow much more accurate and robust estimates of star formation history than are possible using only SDSS data. However, we caution that the UV spectral slope for the majority of galaxies detected in both *GALEX* bands is consistent both with hot stars and with AGN activity. Additional information, such as spatially resolved FUV emission or X-ray, infrared, and radio data, is needed before blue *GALEX* UV colors can be unambiguously interpreted as a sign of recent star formation. For example, Yi et al. (2005) interpreted the *GALEX* detections of 63 elliptical galaxies from an SDSS sample constructed by Bernardi et al. (2003) as evidence for recent star formation. However, as their Figure 3 shows, all 63 of those galaxies have $f - n > 0$ (or $M_f - M_r > M_n - M_r$ in their nomenclature). Our work suggests that, at least in principle, their UV emission may instead reveal low-level AGN activity.

Similarly to Yi et al., Rich et al. (2005) analyze a sample of ∼1000 early-type *GALEX*-SDSS galaxies with redshifts <0.2. They select a subsample of 172 quiescent early-type galaxies by excluding all those with any evidence for non-early-type morphology, star formation, or AGN activity (using emission lines) and point out a surprisingly large range of the $f - r$ color (from ∼3 to ∼8). We find that the observed range of the $f - r$ color can be explained by a small contribution of AGN-like emission to an otherwise normal ("old, red, and dead") elliptical galaxy. For example, assume that an AGN-like SED with $f - n = 0$ and $n - r = 0$ is added to an elliptical galaxy SED with $f - n = 2$ and $n - r = 6$ (Gil de Paz et al. 2005), such that the

AGN contribution to the r-band flux is 1%. The AGN contribution to the overall flux is then 70% in the n band and 94% in the f band. That is, the $f - n$ color is dominated by the AGN contribution and becomes 0.30 (with $f - r = 4.9$). The addition of such low-level AGN emission would likely go undetected in SDSS spectra.

We have used two special-purpose analysis pipelines developed by Tremonti et al. (2004) and Hao et al. (2005) to model and subtract the stellar continuum and measure the residual emission lines in such composite AGN + galaxy spectra. Both codes produce comparable results: the addition of an AGN-like SED with the continuum contribution of 1% in the r band produces a signal-to-noise ratio (S/N) for the Hα emission line >3 in 25% of galaxies and >5 in only 2% of galaxies. When the S/N cutoff is imposed on other lines needed to construct the BPT diagram (Baldwin et al. 1981), such AGN emission is practically unnoticeable in SDSS spectra, although it dominates the *GALEX* flux measurements. Hence, the UV emission from quiescent elliptical galaxies discussed by Rich et al. (2005) could simply be due to low-level AGN activity.

From our analysis of the UV colors of the low-redshift QSOs and the hottest stars detected by SDSS, we find that, in the absence of additional information, the only robust criterion to avoid contamination by AGNs is to require $f - n < 0$ (which, of course, biases the sample toward the youngest starbursts). Indeed, M. Obrić et al. (2005, in preparation) use emission-line strengths to separate star-forming galaxies from AGNs in a sample of main SDSS spectroscopic galaxies detected by *GALEX* and find that the median $f - n$ colors are 0.1 for star-forming galaxies and 0.5 for AGNs, in good agreement with the analysis presented here.

It should be noted that it is not obvious what exactly the $f - n$ color measures. For example, Seibert et al. (2005b) tested the canonical UV color-attenuation (IRX-β) relation for starburst galaxies with a sample of *GALEX* and *Infrared Astronomical Satellite* galaxies and found that it consistently overestimates the attenuation they derive from their sample by half a magnitude. While $f - n$ is certainly expected to be affected by dust attenuation (e.g., Kong et al. 2004; Buat et al. 2005), the distribution of galaxies in the $f - z$ versus $f - n$ diagram implies that the ages of the dominant stellar populations and the corresponding star formation rates must play a significant role in determining the color of a galaxy (as opposed to simply reflecting a varying degree of reddening of one and the same intrinsic stellar population in different galaxies).

Finally, models have some difficulties producing $f - n$ colors at the extreme blue edge $f - n < -0.5$ (e.g., Bianchi et al. 2005). While this discrepancy could, of course, point to suspect observations (e.g., non-Gaussian photometric errors), the modeling of FUV colors of galaxies is notoriously difficult due to the unknown spatial distribution of dust and the poorly constrained dust opacity in this wavelength range. Furthermore, the observed colors of hot stars in our Galaxy do extend all the way to $f - n < -0.5$. In any case, we emphasize that most of our conclusions regarding the nature of *GALEX* sources are model-independent; for example, those that pertain to galaxies are based on the comparison of galaxy colors with those observed for Galactic sources and quasars using the same bands and the same instruments.

REFERENCES

Abazajian, K., et al. 2005, AJ, 129, 1755
Baldwin, J., Phillips, M., & Terlevich, R. 1981, PASP, 93, 5
Becker, R. H., White, R. L., & Helfand, D. J. 1995, ApJ, 450, 559
Bernardi, M., et al. 2003, AJ, 125, 1817
Bertin, E., & Arnouts, S. 1996, A&AS, 117, 393
Bianchi, L., et al. 2005, ApJ, 619, L27
Buat, V., et al. 2005, ApJ, 619, L51
Calzetti, D., Kinney, A. L., & Storchi-Bergmann, T. 1994, ApJ, 429, 582
Cardelli, J. A., Clayton, G. C., & Mathis, J. S. 1989, ApJ, 345, 245
Elvis, M., et al. 1994, ApJS, 95, 1
Fan, X. 1999, AJ, 117, 2528
Finlator, K., et al. 2000, AJ, 120, 2615
Fukugita, M., Ichikawa, T., Gunn, J. E., Doi, M., Shimasaku, K., & Schneider, D. P. 1996, AJ, 111, 1748
Gil de Paz, A., et al. 2005, ApJ, 619, L115
Gunn, J. E., et al. 1998, AJ, 116, 3040
Hao, L., et al. 2005, AJ, 129, 1783
Hibbard, J. E., et al. 2005, ApJ, 619, L87
Høg, E., et al. 2000, A&A, 357, 367
Hogg, D. W., Finkbeiner, D. P., Schlegel, D. J., & Gunn, J. E. 2001, AJ, 122, 2129
Ivezić, Ž., et al. 2002, in IAU Colloq. 184, AGN Surveys, ed. R. F. Green, E. Ye. Khachikian, & D. B. Sanders (ASP Conf. Ser. 284; San Francisco: ASP), 137
———. 2004, Astron. Nachr., 325, 583

Kong, X., et al. 2004, MNRAS, 349, 769
Lupton, R. H., Ivezić, Ž., Gunn, J. E., Knapp, G. R., Strauss, M. A., & Yasuda, N. 2002, Proc. SPIE, 4836, 350
Martin, D. C., et al. 2005, ApJ, 619, L1
Morrissey, P., et al. 2005, ApJ, 619, L7
Pier, J. R., Munn, J. A., Hindsley, R. B., Hennesy, G. S., Kent, S. M., Lupton, R. H., & Ivezić, Ž. 2003, AJ, 125, 1559
Pourbaix, D., Ivezić, Ž., Knapp, G. R., Gunn, J. E., & Lupton, R. H. 2004, A&A, 423, 755
Rich, R. M., et al. 2005, ApJ, 619, L107
Richards, G. T., et al. 2001, AJ, 121, 2308
———. 2002, AJ, 123, 2945
Salim, S., et al. 2005, ApJ, 619, L39
Schlegel, D., Finkbeiner, D. P., & Davis, M. 1998, ApJ, 500, 525
Seibert, M., et al. 2005a, ApJ, 619, L23
———. 2005b, ApJ, 619, L55
Smith, J. A., et al. 2002, AJ, 123, 2121
Smolčić, V., et al. 2004, ApJ, 615, L141
Stoughton, C., et al. 2002, AJ, 123, 485
Strateva, I., et al. 2001, AJ, 122, 1861
Strauss, M. A., et al. 2002, AJ, 124, 1810
Thilker, D. A., et al. 2005, ApJ, 619, L79
Tremonti, C. A., et al. 2004, ApJ, 613, 898
Yi, S., et al. 2005, ApJ, 619, L111
York, D. G., et al. 2000, AJ, 120, 1579